J. Chem. Sci. (2020) 132:68
https://doi.org/10.1007/s12039-020-01778-1

REGULAR ARTICLE

Copper oxide immobilized clay nano architectures as an efficient electrochemical sensing platform for hydrogen peroxide

DHARMENDRA KUMAR YADAV[a], VELLAICHAMY GANESAN[a,*], RUPALI GUPTA[a], MAMTA YADAV[a], PIYUSH KUMAR SONKAR[a] and PANKAJ KUMAR RASTOGI[b]
[a]Department of Chemistry, Institute of Science, Banaras Hindu University, Varanasi, Uttar Pradesh 221 005, India
[b]Department of Chemistry, GLA University, Mathura, Uttar Pradesh 284 401, India
E-mail: velganesh@yahoo.com; velgan@bhu.ac.in

MS received 13 December 2019; revised 6 February 2020; accepted 9 February 2020

Abstract. An electrochemical sensor for hydrogen peroxide (H_2O_2) present in face bleach cream is fabricated using a composite based on bentonite (Bt) clay and copper oxide (CuO) nanoparticles (CuO-Bt). The CuO nanoparticles' immobilization into Bt was carried out by a two-step process in which Cu^{2+} is ion-exchanged into Bt layers (Cu^{2+}-Bt) in the first step followed by the chemical reaction of NaOH with Cu^{2+}-Bt in the second step to get the target material, CuO nanoparticles immobilized Bt (CuO-Bt). The successful immobilization of CuO nanoparticles into Bt is investigated by a variety of techniques like scanning electron microscopy, transmission electron microscopy, FT-IR spectroscopy, UV-Vis spectroscopy, and electrochemical methods. The CuO-Bt composite is coated on a glassy carbon electrode and used as a selective electrochemical sensing platform for the determination of H_2O_2 based on the significant electrocatalytic property of CuO-Bt towards the H_2O_2 oxidation. This amperometric electrochemical sensor shows two linear detection ranges (5–50 μM and 50–10000 μM) with a limit of detection of 4.9 μM. The sensitivity is calculated to be 0.06 μA μM^{-1} cm^{-2}. This electrochemical sensor exhibits high selectivity, stability, and practical applicability for the H_2O_2 determination in real samples.

Keywords. Electrocatalysis; copper oxide nanoparticles; amperometry; hydrogen peroxide; bleach cream; bentonite; electrochemical sensor.

1. Introduction

Clay-based electrochemical sensing platforms are being studied extensively because of their environment benign nature, ion-exchange properties, and nanostructured layers.[1] These sensing platforms are prepared by drop coating of clay suspension or deposition of a thin film of clay on a conductive surface to enhance the selectivity and sensitivity during the target analyte determination.[2] Bentonite (Bt) clay possesses aluminium-phyllosilicate layered structure[3] and it has several beneficial properties like efficient intercalation ability, high surface area, proficient adsorption capability, and high ion-exchange capacity.[4] In green chemistry terms, it is more suitable in electrocatalysis and subsequent applications because of its non-toxic and environmentally friendly nature. Clay minerals can stabilize metal nanoparticles (M NPs) and metal oxide nanoparticles and the resulting materials can be used for trace-level analysis of biological or pharmaceutical samples and environmental pollutants.[5–7] They can also resolve the overlapping of signals of electro-active compounds.[8] Copper oxide nanoparticles (CuO NPs) exhibits high efficient antimicrobial activity and chemical stability as compared to metallic copper nanoparticles and CuO NPs is exploited in solar cells, electrochemical sensors, electrochromic devices, and chemotherapy.[9–11] It is also used as an industrial catalyst for the oxidation of carbon monoxide.[12] Accordingly, clay-based electrochemical sensing platforms with immobilized CuO NPs are expected to play a great significance in the

*For correspondence

Electronic supplementary material: The online version of this article (https://doi.org/10.1007/s12039-020-01778-1) contains supplementary material, which is available to authorized users.

Published online: 26 May 2020

determination of hydrogen peroxide (H_2O_2). H_2O_2 is a colorless oxidizing agent and its oxidizing properties are effective in inhibiting (or killing) the growth of microbes to keep the normal cells healthy. Sensitive assay of H_2O_2 is essential in many fields like clinical diagnosis, pharmaceuticals, food processing, environmental monitoring, and human health care issues because of its significant role in many biological or environmental reactions.[13–16] There are a variety of methods for the detection of H_2O_2 such as fluorimetry, spectrophotometry, chromatography, chemiluminescence, and titrimetry.[17–21] Compared with these methods, electrochemical techniques are superior in many ways such as simplicity, high sensitivity, and relatively low-cost. Because of electrode fouling, slow electrode kinetics, and high overpotential during the redox reaction, it is usually difficult to analyze H_2O_2 at conventional electrodes. Therefore, an electrochemical sensor based on the composite of CuO NPs and Bt is reported for the determination of H_2O_2 in this work.

2. Experimental

2.1 *Instrumentation*

Electrochemical studies (cyclic voltammetry (CV), amperometry, etc.) were done with CHI-660C (CH Instruments electrochemical workstation, USA) with a three electrode one compartment system. Glassy carbon (GC) electrode (area 0.07 cm^2) or modified GC electrode as a working electrode, silver/silver chloride (KCl saturated) as a reference electrode, and platinum wire as a counter electrode were used. The absorption spectra were obtained with a UV-vis absorption spectrophotometer (UV 1700 PharmaSpec, Shimadzu). Powder X-ray diffraction (XRD) patterns were recorded with D8 Advance/Discover (Bruker, Germany) in the 2θ range, 10° to 80°. FT-IR spectra of materials were recorded with PerkinElmer spectrometer (Spectrum two, UK). Scanning electron microscopy (SEM) images were obtained from FE-SEM QUANTA 200 (FEI Netherlands) operating at 20 kV. Energy dispersive X-ray analysis (EDAX) was carried out using SEM VEGA 3 TESCAN at 30 kV. Transmission electron microscopy (TEM) images were recorded on TECNAI 20 G^2FEI microscope, operating at 120 kV.

2.2 *Reagents and chemicals*

Bentonite (Bt) clay was purchased from Himedia, India. K_2HPO_4, KH_2PO_4, sodium hydroxide, and H_2O_2 (50% w/w) were purchased from Qualigens. $CuSO_4$ was purchased from Merck, India. Acetic acid and poly(vinyl alcohol) were purchased from S.D. Fine Chemicals, India. All chemicals were used as received unless otherwise mentioned.

2.3 *Synthesis of CuO-Bt*

For the synthesis of CuO-Bt, 1.0 g Bt was dispersed in 100 mL of aqueous 0.2 M copper sulphate solution containing 2.0 mL of acetic acid. The mixture was boiled to reflux and stirred continuously. Sodium hydroxide solution was added to the mixture under the boiling condition. Immediately after the addition of sodium hydroxide, the color of the solution was changed from dull blue to black, however, the stirring and refluxing was continued further for 24 h. The black suspension was centrifuged after 24 h and washed several times with triple distilled water to remove any physically absorbed CuO and excess ions. The product was dried in an oven at 60 °C.

2.4 *Construction of electrochemical sensing platforms*

A colloidal suspension (0.5%) of Bt or CuO-Bt material was prepared with 0.01% poly(vinyl alcohol) in triple distilled water. The colloidal suspension of the material (5 μL) was drop-coated on the surface of a vertically mounted GC electrode and allowed to dry overnight. Depending upon the material coated, the sensing platform is represented as GC/Bt or GC/CuO-Bt.

3. Results and Discussion

3.1 *Characterization of the materials*

The SEM and TEM images of Bt and CuO-Bt materials are shown in Figure 1. It can be seen that the surface morphology of Bt shows a flatter surface and a clear outline in Figure 1a. The SEM image of CuO-Bt demonstrates that the CuO is grown with different shapes (including spherical shape) on the surface of Bt uniformly (Figure 1b). The TEM image of CuO-Bt shows a slight variation in morphology as compared to Bt images (Figure 1c and 1d). Spherical CuO NPs with a size of 90-125 nm is clearly observed on the surface of Bt (Figure 1d and Figure S1, Supplementary Information). EDAX and elemental mapping of Bt and CuO-Bt are shown in Figures S2 and S3 (Supplementary Information), respectively. EDAX spectrum of Bt shows peaks also due to the elements like K, Ti, Fe, and Mg which may be attributed to the presence of small amounts of impurities in their ionic form as expected.[1–7,24,25] EDAX spectrum of CuO-Bt shows peaks mainly due to Cu, indicating that the ionic impurities originally present in the Bt is removed during the CuO-Bt synthesis. The presence of peak for Cu in the EDAX demonstrates the successful integration of CuO NPs onto the Bt matrix. Elemental

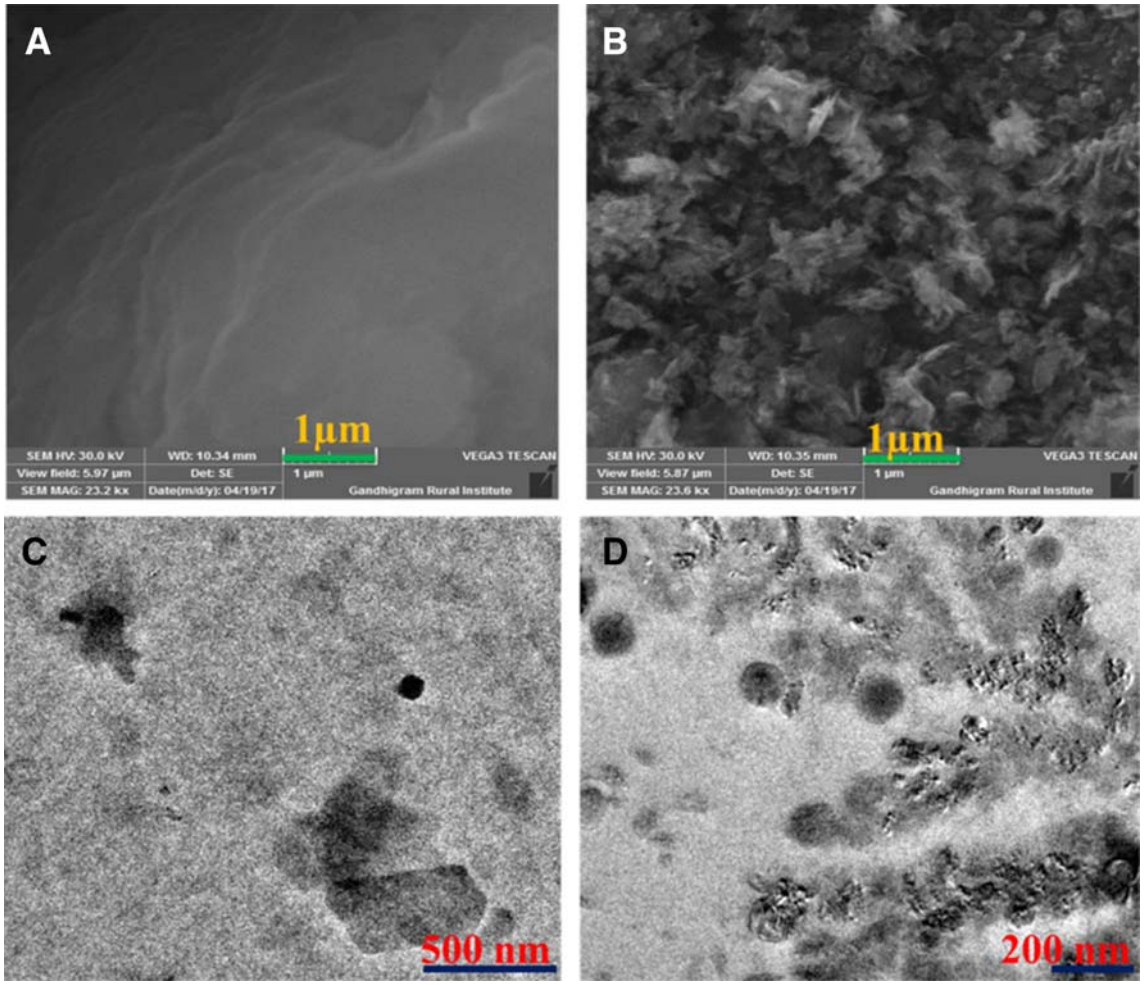

Figure 1. SEM (a and b) and TEM (c and d) images of Bt (a and c) and CuO-Bt (b and d).

mappings of Bt and CuO-Bt show that the elements (C, O, Si, and Al for Bt and C, O, Si, Al, and Cu for CuO-Bt) are distributed throughout the material uniformly.

Figure 2A shows the FT-IR spectra of Bt and CuO-Bt materials. Absorptions at 915, 1035, 1119, and 3690 cm^{-1} are attributed to the characteristic vibrations of Bt. The band observed at 915 cm^{-1} can be assigned to the OH bending vibration of Al-OH. The characteristic peaks at 1035 and 1119 cm^{-1} are ascribed to Si-O out-of-plane and in-plane stretching vibrations, respectively. Absorptions at 3425 and 1634 cm^{-1} are attributed to H-O-H bending and O-H stretching vibrations, respectively. Bands appear at 471 and 531 cm^{-1} in the CuO-Bt material can be ascribed to the vibration of Cu-O bond. Thus, the FT-IR spectra confirm the formation of CuO NPs on Bt.[22–24]

Figure 2B shows the XRD patterns of Bt and CuO-Bt. The characteristic XRD peaks of Bt are found at 2θ values 19.6°, 20.7°, 26.5°, 36.5°, 39.1°, 50.1°, 61.8°, and 68.1°.[25] CuO-Bt material reveals all the peaks as observed in Bt with some additional peaks which can be assigned to CuO NPs. The CuO-Bt shows additional intense peaks for CuO NPs at 2θ values 32.5°, 35.5°, 38.7°, 48.6°, 53.6°, 58.2°, 66.1° and 74.9° which correspond to (110), (111), (−111), (20-2), (020), (202), (220), and (004) planes, respectively.[26] Thus, the XRD patterns confirm the crystalline nature of CuO NPs and its integration with Bt. The presence of unaltered Bt diffraction peaks in the CuO-Bt material indicates that there are no changes in the basic structure of Bt after the incorporation of CuO. Figure 3A shows the UV-vis absorption spectrum of CuO-Bt. The absorption spectrum of CuO-Bt (colloidal suspension) shows bands at 281 and 356 nm. However, Bt shows an absorption peak at 374 nm only (inset of Figure 3A). The peaks at 356 (observed for CuO-Bt) and 374 nm (observed for Bt) may be assigned to the immovable Fe^{2+} or Fe^{3+} impurities generally present in the clay samples. The small shifts in CuO-Bt may be due to the interaction of Fe^{2+} or

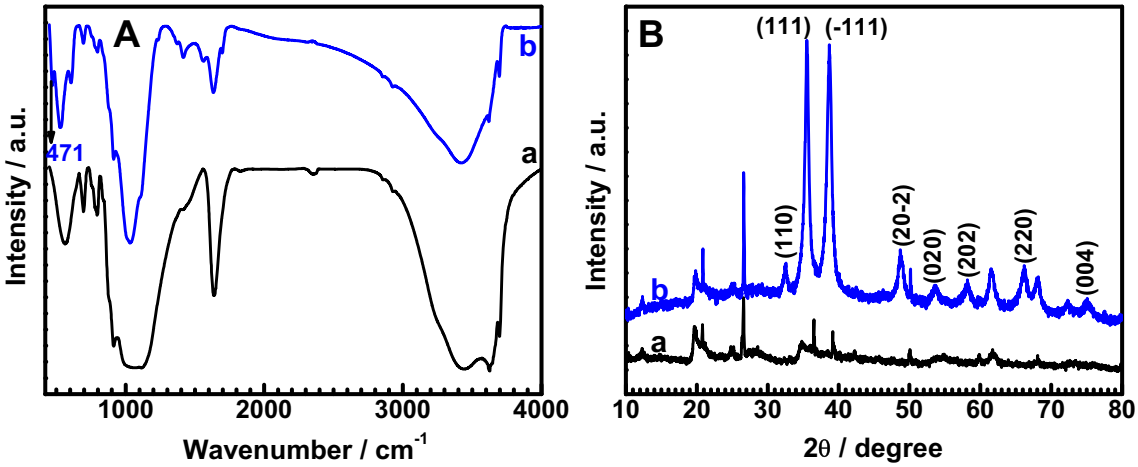

Figure 2. FT-IR spectra (A) and XRD patterns (B) of Bt (a) and CuO-Bt (b) materials.

Fe^{3+} impurities with CuO NPs. The peak at 281 nm observed for CuO-Bt is assigned to the CuO NPs which confirms the integration of CuO with Bt.[27–29]

3.2 *Electrochemical characteristics of GC/CuO-Bt*

Figure 3B shows the CV curves recorded for the GC/CuO-Bt electrode in 0.1 M NaOH at various scan rates. An oxidation peak at −0.15 V (scan rate: 100 mV s^{-1}) and a reduction peak at −0.36 V during the reverse scan is observed which may be attributed to Cu_2O/CuO redox process.[9] The CV of GC/CuO-Bt electrode in 0.1 M NaOH at 10 mV s^{-1} is shown in Figure S4, Supplementary Information. The oxidation and reduction peak currents increase with an increase in the scan rate. The linear relation between the peak currents (anodic *i.e.*, I_{pa} and cathodic *i.e.*, I_{pc}) and scan rates (ν) is shown in the inset of Figure 3B. This linearity between the anodic/cathodic currents with scan rates describes the occurrence of a surface-confined redox phenomenon rather than a diffusion-controlled process at the GC/CuO-Bt electrode surface.[30]

3.3 *Electrocatalytic oxidation of H_2O_2*

The CV responses of GC modified with Bt or CuO-Bt are recorded in 0.1 M NaOH in the absence and presence of 1.0 mM H_2O_2 at 20 mV s^{-1}. In the absence of H_2O_2, GC/Bt shows insignificant anodic

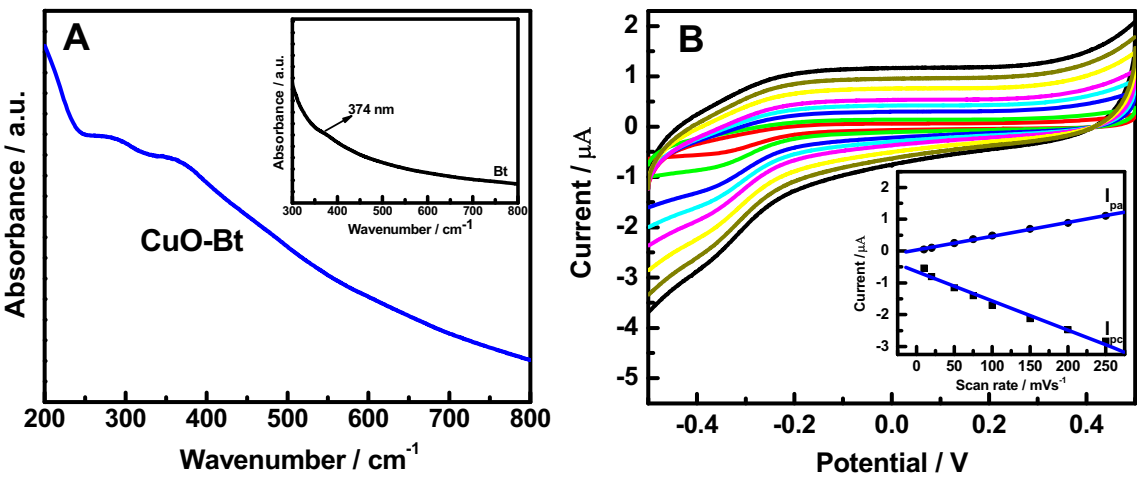

Figure 3. UV-vis spectrum of CuO-Bt (A) and CV responses of GC/CuO-Bt at different scan rates (10, 20, 50, 75, 100, 150, 200, and 250 mV s^{-1}) in 0.1 M NaOH solution (B). Inset of A shows the absorption spectrum of Bt and inset of B shows the graph of current *vs.* scan rate.

current (inset of Figure 4, curve a). In contrast, GC/CuO-Bt (inset of Figure 4, curve b) shows increased anodic current (up to 0.50 V) in the forward scan and a broad cathodic peak at 0.39 V in the reverse scan which may be due to the redox process of Cu^{2+}/Cu^{3+}.[9] Another reduction wave is observed during the cathodic scan at −0.36 V which can be assigned to the reduction of Cu^{2+} to Cu^{+}.[31] Though no peak is observed for the oxidation of Cu^{+} to Cu^{2+} during the anodic scan, at −0.2 V, it is expected that the Cu^{+} get oxidized to Cu^{2+}.[31–33] Similarly, no clear oxidation peak is observed for Cu^{3+} formation at high positive potentials. Upon addition of 1.0 mM H_2O_2, GC/CuO-Bt shows a remarkable increase in the anodic current with a decreased onset potential (0.20 V) for the H_2O_2 oxidation (Figure 4 curve b′). However, at GC/Bt electrode (Figure 4 curve a′) there is a small increase in current due to H_2O_2 oxidation with a high onset potential. The large increase in oxidation current and low onset potential at GC/CuO-Bt electrode demonstrates the superior electrocatalytic performance for the oxidation of H_2O_2 by CuO-Bt material.

3.4 *Amperometric determination of H_2O_2*

The relationship between the current response and H_2O_2 concentration is studied at the GC/CuO-Bt sensing platform by amperometry (at an applied potential 0.15 V) in which H_2O_2 is added successively to the electrolyte solution after certain time intervals. As shown in Figure 5A, upon each addition of H_2O_2,

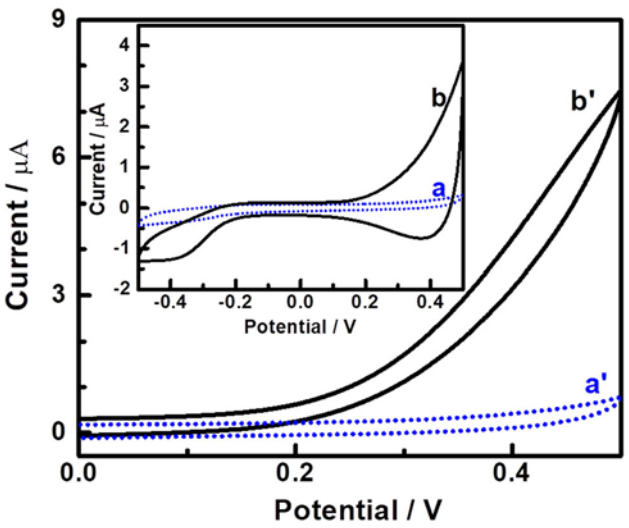

Figure 4. CV curves for the GC/Bt (a and a′) and GC/CuO-Bt (b and b′) in 0.1 M NaOH in the absence (a and b) and presence (a′ and b′) of 1.0 mM H_2O_2 at 20 mV s^{-1} scan rate. Inset shows the CV curves of GC/Bt (a) and GC/CuO-Bt (b) in the absence of H_2O_2.

GC/CuO-Bt sensing platform shows a notable enhancement in current response due to the oxidation of H_2O_2. The observed typical calibration curve is shown in Figure 5B for the determination of H_2O_2. Two linear calibration ranges (5–50 μM and 50–10000 μM) are observed at the sensing platform. The decrease in the slope of the second calibration curve may be due to the kinetic limitations at high concentrations of H_2O_2.[6,7] The sensitivity of the GC/CuO-Bt sensing platform for the determination of H_2O_2 is found to be 0.0098 μA μM^{-1} cm^{-2}. The limit of detection (LOD) is found to be 4.93 μM. A comparison of GC/CuO-Bt performance with other materials/methods is shown in Table 1.[34–44] The H_2O_2 oxidation potential at the GC/CuO-Bt is lower than that observed at several materials/electrodes, such as nanosheets of Ni Fe-layered double hydroxides grown on Ni foam[35] and Ag or Au decorated multi-walled carbon nanotubes.[36] The LOD for the H_2O_2 determination observed at Cu_2O yolk-shell decorated with Pt nanoparticles,[38] Fe-Pt nanoparticles decorated graphene oxide,[40] and composite of graphene/Nafion/Azure I/Au nanoparticles[43] are higher than the present sensor. In addition to the low LOD, the CuO-Bt shows a broad linear calibration range than the chitosan/2D layered double hydroxide composite[34] and CuO NPs on activated pencil graphite electrode.[39] It should also be noted that the present work reports a composite of CuO and clay which could be cost-effective than the other reported materials in Table 1.

3.5 *Interference and stability*

Selectivity is a significant parameter to understand the real applicability and merits of the sensor. Consequently, interferences for the H_2O_2 determination is checked in the presence of some possible interfering species and shown in Figure 6. The selectivity of GC/CuO-Bt sensing platform is assessed by the addition of 200 μM H_2O_2 followed by the successive additions of 1.0 mM of glucose, 200 μM of ascorbic acid, 200 μM of uric acid, and 200 μM of ascorbate (shown in Figure 6A). The recorded amperometric signal signifies a well-defined current response for 200 μM of H_2O_2, whereas a negligible current response is observed during the addition of glucose, ascorbic acid, uric acid, and ascorbate. Thus, the GC/CuO-Bt sensing platform exhibits high selectivity towards the oxidation and subsequent determination of H_2O_2.

The stability of the GC/CuO-Bt sensing platform is examined by oxidizing 300 μM of H_2O_2 for 200 s in 0.1 M NaOH solution (Figure 6B). Immediately after

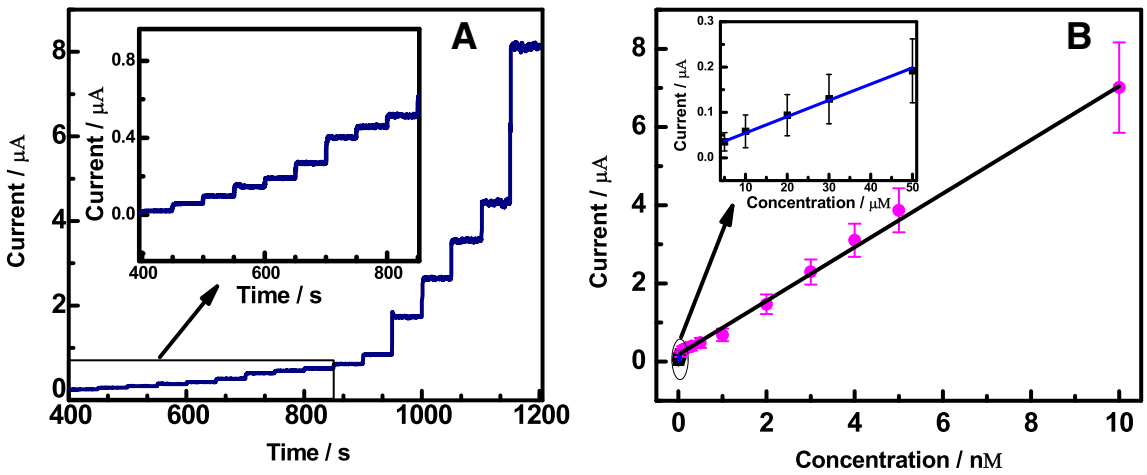

Figure 5. (**A**) Amperometric response of the GC/CuO-Bt sensing platform with successive additions of different concentrations (5, 10, 20, 30, 50, 100, 200, 300, 500, 1000, 2000, 3000, 4000, 5000, and 10000 μM) of H_2O_2 in 0.1 M NaOH. Inset of Figure 5A shows a partial magnification of the amperometric response in the low concentration range. (**B**) The typical calibration curve for the determination of H_2O_2. Inset of Figure 5B shows a partial magnification of the calibration curve in the low concentration range. The error bars are based on ± 1S, where S is the standard deviation of three measurements.

the addition of 300 μM H_2O_2, the current shoots up to a maximum current in less than 2 s due to the oxidation of H_2O_2. After reaching the maximum current, there is no decrease in current for the next 100 s (Figure 6B, curve a). The electrode is removed from the electrolyte solution and stored for the next 30 days in the air at room temperature. After 30 days, the operational response of the same electrode is checked under the identical conditions for the oxidation of 300 μM H_2O_2. The same maximum current is reached exactly in a similar way and retains 100% of its initial value during the first 50 s (Figure 6B, curve b). A small decrease in current is observed after 50 s. From these results, it is clear that the GC/CuO-Bt exhibits long term storage stability.

3.6 *Chronoamperometry*

Chronoamperometry studies were carried out at GC/CuO-Bt to recognize the kinetics of H_2O_2 oxidation at the electrode surface as shown in Figure 7. In the inset of Figure 7, the plot of I_{cat}/I_L *vs.* $t^{1/2}$ is shown and it displays a linear relationship for the oxidation of H_2O_2. The slope of I_{cat}/I_L *vs.* $t^{1/2}$ for 200 μM concentration of H_2O_2 is used to evaluate the catalytic rate constant (k_C). The k_C value of H_2O_2 is calculated to be $2.77 \times 10^4\ M^{-1}\ s^{-1}$ using the equation 1.[45]

$$\frac{I_{cat}}{I_L} = \sqrt{k_C C_b \pi t} \tag{1}$$

where the symbols I_{cat} and I_L represent the catalytic current and limiting current in the presence and absence of H_2O_2, respectively. C_b is the bulk concentration of H_2O_2 and t is the time. The electrocatalytic oxidation (EC' mechanism[46]) of H_2O_2 by CuO-Bt may be given as follows (equations 2 and 3).

$$Cu(II) \rightarrow Cu(III) + e^- \tag{2}$$

$$2Cu(III) + H_2O_2 + 2OH^- \rightarrow 2Cu(II) + O_2 + 2H_2O \text{ (include Bt also)} \tag{3}$$

3.7 *Real sample analysis*

The practical applicability of GC/CuO-Bt is tested for the detection of H_2O_2 in face bleach cream. The face bleach cream (1.0 g) was dissolved in 12 mL of water-ethanol (5:1) mixture. The solution was filtered and the filtrate is quantitatively collected in a beaker. A calculated volume (typically 25 μL) of the filtrate is added to the electrolyte (0.1 M NaOH solution). The amperometric current responses for the face bleach cream alone and also after spiking the electrolyte with two different additions of standard H_2O_2 are measured. The obtained results are reasonable with the relative standard deviation (RSD) values below 7.1% and they are presented in Table 2.

4. Conclusions

In summary, the CuO-Bt composite is successfully synthesized through a hydrothermal route using the mixture of acetic acid, $CuSO_4$, and Bt in the presence of sodium hydroxide at 100 °C. The synthesized

Table 1. Comparison of analytical parameters obtained at GC/CuO-Bt for the H_2O_2 determination with reported methods

Modified electrode/ material[#]	Detection method	Potential (V)	Linear range	Limit of detection (μM)	References
Hemin-catalyzed	HPLC-FD	−0.07	15–300 μM	6.0	17
Copper (I)-DMP complex	UV-visible Spectrophotometric	–	1–100 μM	1.0	18
Triphenylphosphine oxide	HPLC/UV or ceric sulfate titrimetric	–	30–200 μg mL^{-1}	30 μg mL^{-1}	19
Cerate-hydrogen peroxide	Oxidimetry	–	–	–	20
Co(II)-monoethanolamine complex	Chemiluminescence	–	0.2–20 μM	0.1	21
HRP/LDH-CMC	Amperometry	–0.2	20 μM–6.0 mM	12.4	34
NiFe-LDH	Amperometry	0.4	0.5–840 μM	0.5	35
Ag-MWCNT	Amperometry	0.6	0.86–5.8 mM	260	36
Au-MWCNT	Amperometry	0.6	0.86–5.8 mM	260	36
CNTs-MnO_2-TiO_2-Hb/GCE	Amperometry	− 0.339	0.1–200 μM	0.024	37
y-s Pt–Cu_2O/Nafion/GCE	Amperometry	− 0.25	10 μM–6.0 mM and 6.0 mM–16 mM	10.3	38
CuO/APGE	DPV	0.05	5 μM–1.6 mM	0.21	39
FePt/GO	UV-visible	–	30 μM–0.5 mM	22	40
Nafion/GO-Au NPs/ITO	DPV	–	0.01 μM–10 mM	0.0019	41
Cu-TDPAT-nERGO/GCE	Amperometry	− 0.35	4.0 μM–12 mM	0.17	42
Graphene/Nafion/AzI/AuNPs/GCE	Amperometry	− 0.2	30 μM–5.0 mM	10	43
Ensembles of nano-Pt	Amperometry	0.5	42 nM–0.16 mM	0.042	44
GC/CuO-Bt	Amperometry	0.15	5.0–50 μM and 50 μM–10 mM	4.93	This work

[#]FD = Fluorescence detection; DMP = 2,9-dimethyl-l,l0-phenanthroline; HPLC = High-performance liquid chromatography; HRP = horseradish peroxidase; LDH = Layered double hydroxide; CMC = Carboxymethyl chitosan; MWCNT = Multi-walled carbon nanotubes; CNTs = Carbon nanotubes; Hb = Hemoglobin; GCE = Glassy carbon electrode; y-s = yolk–shell; APGE = Activated pencil graphite electrode; ITO = Indium tin oxide; TDPAT = 2,4,6-tris(3,5-dicarboxylpheny-lamino)-1,3,5-triazine; nERGO = nanosized electrochemically reduced graphene oxide; AzI = Azure I; DPV = differential pulse voltammetry.

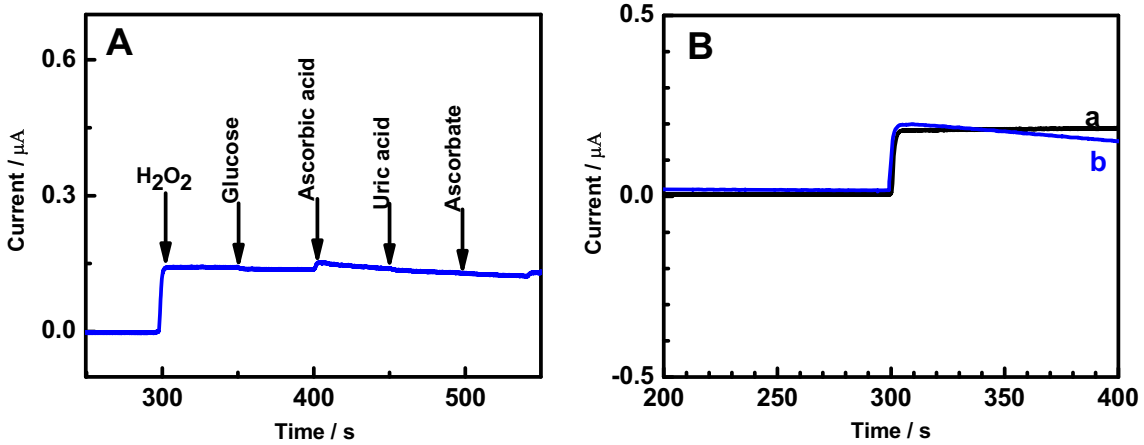

Figure 6. (**A**) i − t Amperometric response at GC/CuO-Bt upon successive additions of 200 μM H_2O_2, 1.0 mM glucose, 200 μM ascorbic acid, 200 μM uric acid, and 200 μM ascorbate in a 0.1 M NaOH solution. (**B**) The amperometric response at GC/CuO-Bt for 0.3 mM H_2O_2 oxidation measured for a long period of time (500 s) before and after 30 days of storage (a and b, respectively).

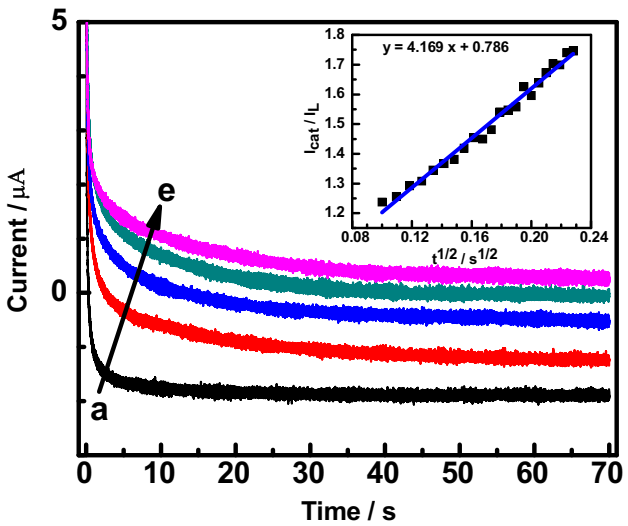

Figure 7. Chronoamperograms recorded at the GC/CuO-Bt in the presence of H_2O_2 (a to e; 0, 100, 200, 300, and 400 μM). Inset shows the plot of I_{cat}/I_L *vs.* $t^{1/2}$ obtained from the chronoamperograms.

Table 2. Recovery analysis of H_2O_2 present in face bleach cream using the GC/CuO-Bt electrode.

Sample	Analyte	Added (μM)	Found (μM)	Recovery* (%)	RSD** (%)
Face bleach cream (Dabur India Ltd.)	H_2O_2	0.0	598.6	–	5.9
		100.0	690.7	98.9	6.5
		200.0	892.5	99.3	7.1

*Recovery (%) = $[Analyte]_{found}/[Analyte]_{added} \times 100$

**RSD is based on the three measurements.

material is characterized by physicochemical and electrochemical methods. The CuO-Bt modified GC is applied for the detection of H_2O_2 and it exhibits high sensitivity, low detection limit, and extended linear calibration range from 5 μM to 10.0 mM. The CuO-Bt material is successfully applied for the determination of H_2O_2 in a face bleach cream sample. Therefore, the CuO-Bt material could be a promising material for the electrochemical sensing of H_2O_2 in the samples with simple matrixes.

Supplementary Information (SI)

Figure S1–S4 are available at www.ias.ac.in/chemsci.

Acknowledgements

Financial support from DST-ASEAN (IMRC/AISTDF/R&D/P-16/2018), New Delhi is gratefully acknowledged. DKY acknowledges UGC for senior research fellowship (SRF). We thank Dr. S.A. John, Gandhigram Rural Institute for SEM and EDAX studies. We thank Ms. Anindita Dutta for her assistance during the initial stage of this study in the synthesis and characterization of the material and the electrocatalytic determination H_2O_2.

References

1. Fitch A 1990 Clay-modified electrodes: a review *Clays Clay Miner.* **38** 391
2. Mousty C 2004 Sensors and biosensors based on clay-modified electrodes-new trends *Appl. Clay Sci.* **27** 159
3. Vaccari A 1998 Preparation and catalytic properties of cationic and anionic clays Angelo Vaccari *Catal. Today* **41** 53

4. Vaccari A 1999 Clays and catalysis: a promising future *Appl. Clay Sci.* **14** 161
5. Rastogi P K, Yadav D K, Pandey S, Ganesan V, Sonkar P K and Gupta R 2016 Synthesis and characterization of gold nanoparticles incorporated bentonite clay for electrocatalytic sensing of arsenic(III) *J. Chem. Sci.* **128** 349
6. Yadav D K, Gupta R, Ganesan V, Sonkar P K and Rastogi P K 2016 Electrochemical sensing platform for hydrogen peroxide determination at low reduction potential using silver nanoparticle-incorporated bentonite clay *J. Appl. Electrochem*. **46** 103
7. Yadav D K, Gupta R, Ganesan V and Sonkar P K 2017 Individual and simultaneous voltammetric determination of ascorbic acid, uric acid and folic acid by using a glassy carbon electrode modified with gold nanoparticles linked to bentonite via cysteine groups *Microchim. Acta* **184** 1951
8. Chiang C Y, Aroh K and Ehrman S H 2012 Copper oxide nanoparticle made by flame spray pyrolysis for photoelectrochemical water splitting-Part I. CuO nanoparticle preparation *Int. J. Hydrogen Energy* **37** 4871
9. Wu D, Xu Z, Zhang T, Shao Y, Xi P, Li H and Xu C 2016 Cu_2O/CuO@rGO heterostructure derived from metal–organic-frameworks as an advanced electrocatalyst for non-enzymatic electrochemical H_2O_2 sensor *RSC Adv.* **6** 103116
10. Sankar R, Maheswari R, Karthik S, Shivashangari K S and Ravikumar V 2014 Anticancer activity of Ficus religiosa engineered copper oxide nanoparticles *Mater. Sci. Eng. C* **44** 234
11. Maleh H K, Amini F, Akbari A and Shojaei M 2017 Amplified electrochemical sensor employing CuO/SWCNTs and 1-butyl-3-methylimidazolium hexafluorophosphate for selective analysis of sulfisoxazole in the presence of folic acid *J. Colloid Interface Sci.* **495** 61
12. White B, Yin M, Hall A, Le D, Stolbov S, Rahman T, Turro N and Brien S 2006 Complete CO oxidation over Cu_2O nanoparticles supported on silica gel *Nano Lett*. **6** 2095
13. Gupta R, Singh P, Koch B, Ganesan V, Rastogi P K, Yadav D K and Sonkar P K 2018 Palladium nanoparticles supported on mesoporous silica microspheres for enzyme-free amperometric detection of H_2O_2 released from living cells *Sens. Actuat. B-Chem.* **276** 517
14. Chen W, Chen J, Feng Y B, Hong L, Chen Q Y, Wu L F, Lin X H and Xia X H 2012 Peroxidase-like activity of water-soluble cupric oxide nanoparticles and its analytical application for detection of hydrogen peroxide and glucose *Analyst* **137** 1706
15. Song M J, Hwang S W and Whang D 2010 Non-enzymatic electrochemical CuO nanoflowers sensor for hydrogen peroxide detection *Talanta* **80** 1648
16. Wu D, Xu Z, Zhang T, Shao Y, Xi P, Li H and Xu C 2016 Cu_2O/CuO@rGO hetero structure derived from metal-organic-frameworks as an advanced electrocatalyst for non-enzymatic electrochemical H_2O_2 sensor *RSC Adv*. **6** 103116
17. Tarvin M, McCord B, Mount K, Sherlach K and Miller M L 2010 Optimization of two methods for the analysis of hydrogen peroxide: High performance liquid chromatography with fluorescence detection and high performance liquid chromatography with electrochemical detection in direct current mode *J. Chromatogr. A* **1217** 7564
18. Baga A N, Johnson G R A, Nazhat N B and Nazhat R A S 1988 A simple spectrophotometric determination of hydrogen peroxide at low concentrations in aqueous solution *Anal. Chim. Acta* **204** 349
19. Gimeno P, Bousquet C, Lassu N, Maggio A F, Civade C, Brenier C and Lempereur L 2015 High-performance liquid chromatography method for the determination of hydrogen peroxide present or released in teeth bleaching kits and hair cosmetic products *J. Pharm. Biomed. Anal.* **107** 386
20. Hurdis E C and Romeyn H 1954 Accuracy of determination of hydrogen peroxide by cerate oxidimetry *Anal. Chem*. **26** 320
21. Hanaoka S, Lin J M and Yamada M 2001 Chemiluminescent flow sensor for H_2O_2 based on the decomposition of H_2O_2 catalyzed by cobalt(II)-ethanolamine complex immobilized on resin *Anal. Chim. Acta* **426** 57
22. Kayani Z N, Umer M, Riaz S and Naseem S 2015 Characterization of Copper Oxide Nanoparticles Fabricated by the Sol-Gel Method *J. Electron. Mater.* **44** 3704
23. Srivastava S, Kumar M, Agrawal A and Dwivedi S K 2013 Synthesis and characterisation of copper oxide nanoparticles *J. Appl. Phys.* **5** 61
24. Azad U P, Turllapati S, Rastogi P K and Ganesan V 2014 Tris(1,10-phenanthroline)iron(II)-bentonite film as efficient electrochemical sensing platform for nitrite determination *Electrochim. Acta* **127** 193
25. Mallakpour S and Dinari M 2011 Preparation and characterization of new organoclays using natural amino acids and Cloisite Na^+ *Appl. Clay Sci*. **51** 353
26. Felix S, Chakkravarthy R B P and Grace A N 2015 Microwave assisted synthesis of copper oxide and its application in electrochemical sensing *Mater. Sci. Eng.* **73** 012115
27. Sankar R, Maheswari R, Karthik S, Shivashangari K S and Ravikumar V 2014 Anticancer activity of Ficus religiosa engineered copper oxide nanoparticles *Mater. Sci. Eng. C* **44** 234
28. Yin M, Wu C K, Lou Y, Burda C, Koberstein J T, Zhu Y and Brien S 2005 Copper oxide nanocrystals *J. Am. Chem. Soc.* **127** 9506
29. Chen W, Hong L, Liu A L, Liu J Q, Lin X H, Xia X H 2012 Enhanced chemiluminescence of the luminol-hydrogen peroxide system by colloidal cupric oxide nanoparticles as peroxidase mimic *Talanta* **99** 643
30. Huo H, Guo C, Li G, Han X and Xu C 2014 Reticular-vein-like Cu@Cu_2O/reduced graphene oxide nanocomposites for a non-enzymatic glucose sensor *RSC Adv*. **4** 20459
31. Bellakhal N, Draou K and Brisset J L 1997 Electrochemical investigation of copper oxide films formed by oxygen plasma treatment *J. Appl. Electrochem*. **27** 414
32. Vazquez M V, Sanchez S R, Calvo E J and Schiffrin D J 1994 The electrochemical reduction of hydrogen peroxide on polycrystalline copper in borax buffer *J. Electroanal. Chem.* **374** 179
33. Casella I G, Cataldi T R I, Guerrieri A and Desimoni E 1996 Copper dispersed into polyaniline films as an

amperometric sensor in alkaline solutions of amino acids and polyhydric compounds *Anal. Chim. Acta* **335** 217
34. Yuan J, Xu S, Zeng H Y, Cao X, Pan A D, Xiao G F and Ding P X 2018 Hydrogen peroxide biosensor based on chitosan/2D layered double hydroxide composite for the determination of H_2O_2 *Bioelectrochemistry* **123** 94
35. You T, Qing C, Quanhui L, Guolin Y, Hongtao G, Gang C and Chengjun D 2018 *Surf. Interfac.* **12** 102
36. Guzsvany V, Vajdle O, Gurdeljevic M and Konya Z 2018 Highly sensitive nonenzymatic H_2O_2 sensor based on Ni Fe-layered double hydroxides nanosheets grown on Ni foam *Top. Catal*. **61** 1350
37. Liu C, Shi E, Yao J and Peng R 2018 Ag or Au nanoparticles decorated multiwalled carbon nanotubes coated carbon paste electrodes for amperometric determination of H_2O_2 *Int. J. Electrochem. Sci*. **13** 5253
38. Lv J, Kong C, Liu K, Yin L, Ma B, Zhang X, Yang S and Yang Z 2018 Promotion effects of CNTs-MnO_2 nanowires-composite on direct electron transfer of hemoglobin for amperometric H_2O_2 determination *Chem. Commun*. **54** 8458
39. Kamyabi M A and Hajari N 2017 Surfactant-free synthesis of Cu_2O yolk-shell cubes decorated with Pt nanoparticles for enhanced H_2O_2 detection *J. Braz. Chem. Soc.* **28** 808
40. Chen M, Yang B, Zhu J, Liu H, Zhang X, Zheng X and Liu Q 2018 FePt nanoparticles-decorated graphene oxide nanosheets as enhanced peroxidase mimics for sensitive response to H_2O_2 *Mater. Sci. Eng. C* **90** 610
41. Jin G H, Ko E, Kim M K, Tran V K, Son S E, Geng Y, Hur W and Seong G H 2018 Graphene oxide-gold nanozyme for highly sensitive electrochemical detection of hydrogen peroxide *Sens. Actuat. B Chem*. **274** 201
42. Li C, Zhang T, Zhao J, Liu H, Zheng B, Gu Y, Yan X, Li Y, Lu N, Zhang Z and Feng G 2017 Boosted sensor performance by surface modification of bifunctional rht-type metal-organic framework with nanosized electrochemically reduced graphene oxide *ACS Appl. Mater. Interfaces* **9** 2984
43. Zhang Y, Liu Y, He J, Pang P, Gao Y and Hu Q 2013 Electrochemical behavior of graphene/Nafion/Azure I/Au nanoparticles composites modified glass carbon electrode and its application as nonenzymatic hydrogen peroxide sensor *Electrochim. Acta* **90** 550
44. Raj C R and Chakraborty S 2009 Pt nanoparticle-based highly sensitive platform for the enzyme-free amperometric sensing of H_2O_2 *Biosens. Bioelectron.***24** 3264
45. Gupta R and Ganesan V 2015 Gold nanoparticles impregnated mesoporous silica spheres for simultaneous and selective determination of uric acid and ascorbic acid *Sens. Actuat. B Chem*. **219** 139
46. Bard A J and Faulkner L R 1980 *Electrochemical Methods; Fundamentals, Applications* (New York: Wiley)